

See discussions, stats, and author profiles for this publication at: <https://www.researchgate.net/publication/279863455>

Electronic Transport via Homo-peptides: The Role of Side Chains and Secondary Structure

ARTICLE *in* JOURNAL OF THE AMERICAN CHEMICAL SOCIETY · JULY 2015

Impact Factor: 12.11 · DOI: 10.1021/jacs.5b03933 · Source: PubMed

CITATION

1

READS

46

10 AUTHORS, INCLUDING:



[Sivan Refaely-Abramson](#)

University of California, Berkeley

9 PUBLICATIONS 361 CITATIONS

[SEE PROFILE](#)



[Piyush Agrawal](#)

Empa - Swiss Federal Laboratories for Material...

3 PUBLICATIONS 14 CITATIONS

[SEE PROFILE](#)



[Mordechai Sheves](#)

Weizmann Institute of Science

256 PUBLICATIONS 5,143 CITATIONS

[SEE PROFILE](#)



[David Cahen](#)

Weizmann Institute of Science

479 PUBLICATIONS 13,494 CITATIONS

[SEE PROFILE](#)

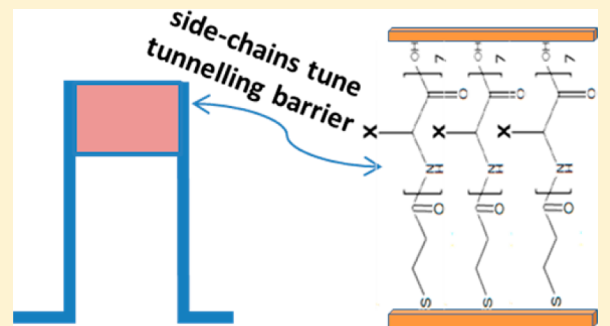
Electronic Transport via Homopeptides: The Role of Side Chains and Secondary Structure

Lior Sepunaru,^{†,‡,§} Sivan Refaelly-Abramson,[†] Robert Lovrinčić,[†] Yulian Gavrilov,[§] Piyush Agrawal,[†] Yaakov Levy,[§] Leeor Kronik,[†] Israel Pecht,^{||} Mordechai Sheves,^{*,‡} and David Cahen^{*,†}

[†]Department of Materials and Interfaces, [‡]Department of Organic Chemistry, [§]Department of Structural Biology, and ^{||}Department of Immunology, Weizmann Institute of Science, Rehovot, 7610001, Israel

Supporting Information

ABSTRACT: Many novel applications in bioelectronics rely on the interaction between biomolecules and electronically conducting substrates. However, crucial knowledge about the relation between electronic transport via peptides and their amino-acid composition is still absent. Here, we report results of electronic transport measurements via several homopeptides as a function of their structural properties and temperature. We demonstrate that the conduction through the peptide depends on its length and secondary structure as well as on the nature of the constituent amino acid and charge of its residue. We support our experimental observations with high-level electronic structure calculations and suggest off-resonance tunneling as the dominant conduction mechanism via extended peptides. Our findings indicate that both peptide composition and structure can affect the efficiency of electronic transport across peptides.



INTRODUCTION

Understanding electronic conduction through biomolecules is crucial for the design of bioelectronics applications. At the same time, it is of great general interest to explore the electron transfer (ET) through proteins, because of its biological importance. While common methods to study ET probe proteins by electrochemical or spectroscopic measurements,^{1–3} a solid-state molecular junction can be used to study the conduction via a protein, placed between two electronically conductive electrodes.^{4–7} In such a device, the electronic transport (ETp) is measured without requiring redox activity of a site within the examined molecule. Proteins are amino acid polymers. Thus, investigating ETp across short constituent peptides presents a necessary step toward understanding the more complex ETp via proteins, while also providing a possibility for introducing high-level electronic structure computations. Sek⁸ and Long et al.⁹ reviewed experimental efforts to investigate both ETp and ET via peptides, respectively, in a systematic manner. Long et al. ended their review with the question: ‘Can it be expected that ET processes operate by the same mechanism in peptides of different amino acid sequences and different secondary structures?’ This question is fundamental for understanding both ET and ETp processes, and the answer to it can shed light on the ET pathways, and to improve the design of bioelectronics devices of interest.

Juhaniiewicz et al.¹⁰ took the first step toward answering the above question in the solid state, by studying a junction composed of a single amino acid (e.g., glycine, alanine, or

proline), linked by cystamine to electrodes. They observed similar conduction for all examined amino acids. In the present work, we take a further step toward answering the above question, by investigating the conduction through a molecular monolayer junction composed of homopeptides, consisting of n repeating identical amino acids. Specifically, we examine three fundamental structural variations: First, we use extended homopeptides of similar length but varying side-chains, to examine the effect of the amino acid composing the homopeptide monolayer on transport. Second, we investigate the role of the homopeptide’s length on ETp, by changing the number of repeating units (i.e., of the amino acids). Third, we compare peptide monolayer junctions with similar length and side-chains but different secondary structure, by examining the difference in transport efficiency between random-structured and helical homopeptides. By this, we address the following questions: Do peptides comprised of different amino acids conduct differently? What is the transport mechanism via the examined homopeptides? What is the role of secondary structure of the peptide in its conduction?

Our investigation is based on measurements of the conduction through a monolayer of homopeptides between gold electrodes,¹¹ as a function of bias voltage and temperature. In addition we measured differential conductance and inelastic electron tunneling spectra (IETS) of the junctions. The experimental setup as well as the procedures for sample

Received: April 16, 2015

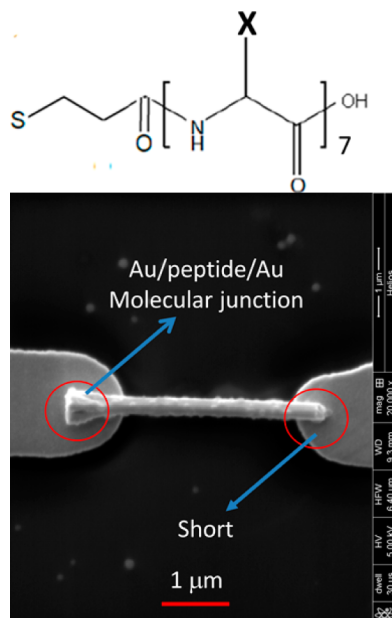
Published: July 6, 2015

preparation are given in the *Supporting Information* (SI). To assist in the interpretation of the experimental results, we use molecular dynamics (MD) and density-functional theory (DFT) simulations that suggest the structure of each examined system. We further explore the gas-phase electronic structure of the examined peptides, using optimally tuned range-separated hybrid (OT-RSH)¹² DFT calculations. These have recently been shown to yield excellent gas-phase highest occupied molecular orbital (HOMO) – lowest unoccupied molecular orbital (LUMO) gaps¹³ as well as frontier energy levels and outer-valence spectra.^{14–16} They therefore avoid the vanishing gaps often encountered in standard DFT calculations of proteins^{17,18} and other highly polar molecules¹⁹ (see SI for computational details).

RESULTS

Conduction of Oligo-Homopeptide Monolayers As a Function of Amino Acid. We first explored ET_p through homopeptide molecular junctions of constant length, while changing the amino acid. Four different homopeptides were investigated, each composed of seven identical amino acids: alanine (Ala), tryptophan (Trp), glutamic acid (Glu), and lysine (Lys). From the results of ellipsometry, infrared spectroscopy, and MD calculations we deduce that all four peptides adopted an extended random conformation, namely their backbone was linearly stretched along the junction (see Table 1 and Figures S1 and S2 in the SI). At the N-terminal of each peptide, a mercaptopropionic acid (MPA) linker was attached (see Scheme 1). The preparation of molecular junctions was done as reported earlier¹¹ and is also described in the SI. The junction contact area was estimated to be $\sim 5000 \text{ nm}^2$ and contained $\sim 5 \times 10^3$ peptides, except for the Ala ones, where the upper bound is about an order of magnitude higher.

Scheme 1. (Top) Hepta Homo-Peptide Model System^a and (Bottom) SEM Scan of a Trapped Au Nanorod That Forms the Mesoscopic Peptide Junction in a Au/Peptide/Au Molecular Junction Configuration



^aA mercaptopropionic acid was used to link the monolayer to a gold substrate.

All monolayers were bound to a Au surface via a Au–S bond. This was confirmed *in situ* (during ET_p measurements), as shown by their symmetric IETS peaks around 270 cm⁻¹ ($\sim 33.5 \text{ mV}$) which correspond to the Au–S vibrational mode (cf. Figure 1a and Video S1 in the SI).²⁰ While low vibrational modes in peptides were observed by ultrafast optical heterodyne-detected Raman-induced Kerr-effect spectroscopy,²¹ the 270 cm⁻¹ peak position was identical for all the peptides and reflects the commonly observed contribution of the contact to the electrode, as reported also by others.²² In addition to the distinct Au–S vibrational mode, two additional IETS peaks were observed for all peptides. The additional peaks correspond to C–H stretching vibrational modes, arising mostly from the MPA linker, and to the side chains of the investigated homopeptide (see Figure S3 for hepta-Trp as an example). All four peptides had a similar length of $25 \pm 2 \text{ Å}$, long enough to allow formation of a sufficiently pinhole-free monolayer and prevent direct current flow between the Au electrodes, but sufficiently short to prevent them from adopting a defined secondary structure. Figure 1b shows the resulting current–voltage curves for junctions of the four peptides (see Summary of Materials and Methods section for full explanation), positioned between the Au substrate bottom contact and a single Au nanorod serving as the top contact. A marked difference in ET_p is found between the different peptide monolayers, with Trp being the best conductor, followed by Lys and Glu (for both the residues were neutral) and with Ala as the poorest conductor ($G_{\text{Trp}} > G_{\text{Lys}} \sim G_{\text{Glu}} > G_{\text{Ala}}$ at 7 K see Figure S3). The current–voltage plots indicate a 20-fold ($G_{\text{Trp}}/G_{\text{Ala}}$) span in conduction via the different homopeptides. These differences cannot be attributed to differences in the density of peptide molecules in the monolayer, assuming close packing (a density that can be derived from their calculated footprint areas; cf. Table S1 in SI), as then the order of conductances would be Ala > Glu ~ Lys > Trp, which is opposite to the order that is found experimentally.

The computed gas-phase HOMO levels of the four examined peptides, shown in Figure 1c, predict the HOMO energy of hepta-Trp to be higher than that of all other examined peptides, -7.4 eV . The HOMO levels of hepta-Ala, hepta-Glu, and hepta-Lys are all at $\sim -9 \text{ eV}$ (see details in Table 1). It is reasonable to assume a similar level of renormalization of the frontier levels from the gas-phase to the solid-state²³ for all examined peptides, because the electrodes and thiol linker groups are the same for the different peptides. For thiols, the interface dipole is such that upon surface binding it shifts occupied levels down in energy with respect to the Fermi energy. This shift was shown to be of the order of 1 eV.²⁴ Further changes are expected to occur due to dipole–dipole interactions between the peptides in the monolayer, depending on the sign and magnitude of the dipole.²⁵ As the overall length of the peptides is similar and as their dipoles are of the same order of magnitude, we do not expect the dipole–dipole interactions to change the observed trend. Altogether, the difference between the gas-phase HOMO levels of the different homopeptides can approximate the trends in the differences between the solid-state HOMO levels of these peptides. (A similar observation can be made for the LUMO levels; see SI Figure S4). Following this assumption, our computations predict a lower barrier height for hepta-Trp than for all other peptides and can hence explain its higher conductance. The reduced fundamental gap is also expressed by fitting our

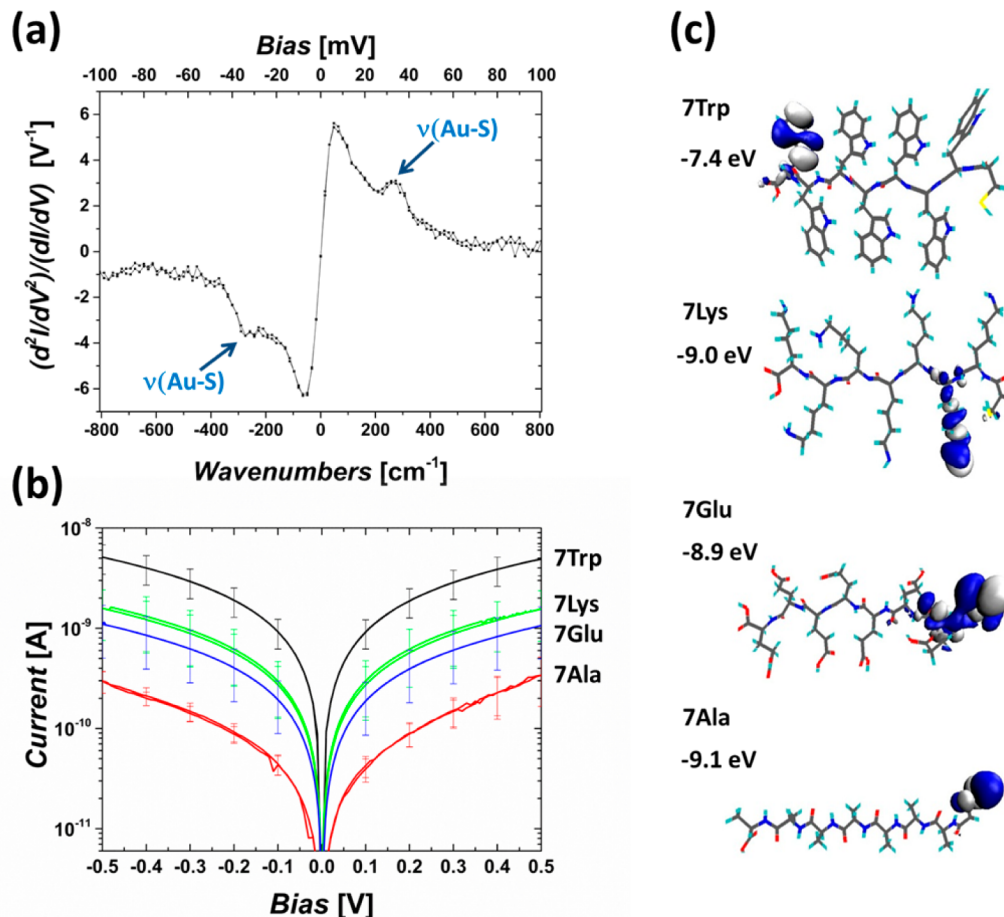


Figure 1. (a) IETS spectrum of a representative (protonated, i.e., uncharged hepta-Glu) Au/peptide/Au junction at 7 K, showing the Au–S vibrational mode at 270 cm^{-1} . (b) Comparison of current–voltage (I – V) characteristics via monolayers of hepta homopeptides of Trp, Lys, Glu, and Ala. The residues of hepta-Lys and hepta-Glu are uncharged (c) The computed value of the HOMO energies for each of the gas-phase hepta-peptides, along with their corresponding orbital densities. The computations were based on the geometries obtained from MD (cf. Figure S2 in the SI). Here and throughout, grey lines represent carbon atoms, red, oxygen atoms, blue- nitrogen atoms, yellow, sulfur atoms, and cyan, hydrogen atoms.

Table 1. Combined Experimental Observations with the Electronic Structure Gas Phase Calculations

peptide	Hepta-Trp	Hepta-Lys	Hepta-Glu	Hepta-Ala	20 mer Ala	20 mer Lys
thickness ^a (Å) (theoretical)	26 ± 2 (23.8)	25 ± 1.5 (25.8)	25 ± 2 (24.9)	24 ± 2 (27.2)	29 ± 2 (28.7)	30 ± 2 (33.7)
current at 0.1 V	$9.2 \pm 2.9 \times 10^{-10}\text{ A}$	$(\text{NH}_2) 3.0 \pm 1.8 \times 10^{-10}\text{ A}$ (NH_3^+) $3 \pm 1.5 \times 10^{-9}\text{ A}$	$(\text{COOH}) 1.9 \pm 1.0 \times 10^{-10}\text{ A}$ (COO^-) $5.8 \pm 2.6 \times 10^{-11}\text{ A}$	$4.2 \pm 1.0 \times 10^{-11}\text{ A}$	$1.6 \pm 0.2 \times 10^{-9}\text{ A}$	$2.4 \pm 0.7 \times 10^{-8}\text{ A}$
HOMO energy in [eV] ^b	-7.4	-9.0	-8.9	-9.1 ^c (-9.8)	-6.6	-6.6

^aMeasured (by ellipsometry) and calculated (edge to edge distance from MD simulations) thicknesses of the peptide monolayers, their corresponding currents at 0.1 V (linear regime of the current-voltage plot), and calculated molecular orbital energies. ^bAll calculations are for molecules in the gas phase. The estimated accuracy for the MO levels is ~ 0.2 eV. ^cThe HOMO level of hepta-Ala is expected to hybridize with the gold surface, making the HOMO-1 orbital at -9.8 eV the frontier MO.

conductance measurement to common theoretical models.^{26,27} From the Simmons model, using the β values that we extracted from the length dependent conductance data (vide infra) or from the Landauer model, we estimate the barrier height for ETp via oligo-Trp to be ~ 0.3 – 0.5 eV (see detailed calculation in SI). We interpret this barrier height to reflect the difference between the Fermi level of the gold electrodes and the nearest peptide orbital energy, an issue that we are currently investigating experimentally by comparing the gas phase results to those from solid state (monolayer on Au surface) by UPS experiments.

The calculated gas-phase HOMO levels of the (uncharged) hepta-Ala, hepta-Lys, and hepta-Glu are very similar, which seemingly disagrees with the experimental observations, from which we would expect hepta-Lys and hepta-Glu to have a considerably higher HOMO level than that of hepta-Ala. To understand the relation between these results and those of the experimental measurements, we turn to investigating the corresponding orbitals of the gas-phase HOMO levels for each one of the homopeptides, also shown in Figure 1c. While the HOMO orbitals of Trp and Lys are highly localized on one of the side-chains, the HOMO level of hepta-Glu is more

delocalized, on both the MPA group and a part of the peptide backbone. For hepta-Ala, the HOMO is highly localized on the MPA group. This may imply that upon adsorption, the hepta-Ala HOMO will hybridize with the energy levels of the Au surface,^{28,29} leaving the HOMO-1 and HOMO-2 orbitals, located ~ 0.7 eV lower in energy, to be the frontier molecular orbitals relevant for transport. The expected energy barrier for conductance would then indeed be lower for hepta-Lys and hepta-Glu than for hepta-Ala.

So far, we have only considered uncharged peptides. However, the NH₂ and COOH groups on the Lys and Glu residues, respectively, maybe protonated and deprotonated, which can affect their electronic structure and, in turn, transport properties. It is therefore interesting to explore the impact of charging on both experimental and computational results. Figure 2 shows the ETp results via protonated and

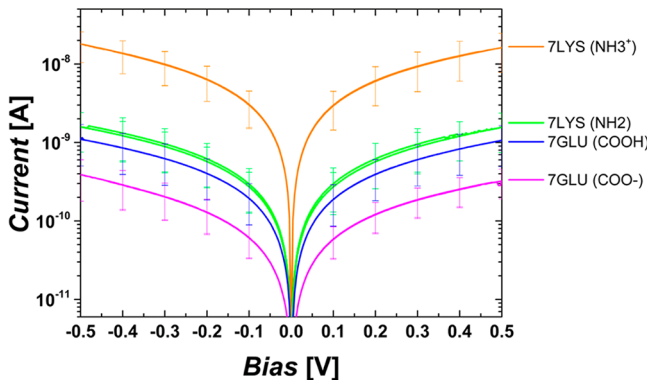


Figure 2. Current–voltage plots of hepta-Lys and hepta-Glu in the respective protonated and deprotonated states of their side chains.

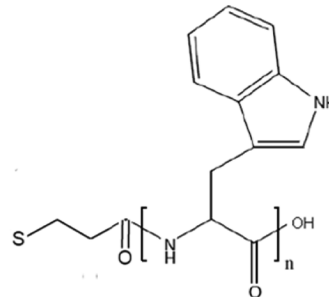
deprotonated hepta-Lys and hepta-Glu, respectively (see SI for experimental details). ETp via the protonated, positively charged hepta-Lys is the highest among all examined hepta-peptides, while ETp via the deprotonated, negatively charged hepta-Glu is comparable to that of hepta-Ala. This high conductance of protonated Lys is consistent with the recent theoretical investigation by Tarakeshwar et al.,³⁰ which predicted that the presence of one protonated Lys residue in hepta-Ala (where one Ala residue is replaced by Lys) would lead to an increase in conduction by nearly 3 orders of magnitude.

We also performed calculations of the electronic structure of these peptides, where three protons were added to side chains 2, 4, and 6 of the hepta-Lys (7LYS-3p) and three removed from the same side-chains of hepta-Glu (7GLU-3dp). Note that in these gas-phase calculations, counterions were not added. We found that the energies of both occupied and unoccupied electronic levels significantly decrease upon protonation (of hepta-Lys) and increase upon deprotonation of (hepta-Glu), as shown in Figure S5 in the SI. Judging by the level alignment alone, this would indicate electron transport through the LUMO, such that transport is enhanced when the level is lowered and suppressed when it is raised. This is perhaps the case for hepta-Lys, but it remains to be confirmed experimentally. For hepta-Glu, current suppression upon deprotonation may also be based on the high localization of the HOMO at the deprotonated sites, which may impede transport via a strong decrease of the coupling to the electrodes. We stress, however, that in this case the computations are but a

model from which various qualitative scenarios can be gleaned, as the counterionic environment may also play an important role.

The Effect of Length on Electronic Transport via Homopeptide Monolayers. To study the relation between the length of the molecular junction and its conductance, we measured the ETp through a homo-Trp molecular junction of different lengths (see Scheme 2). Trp is known to be an

Scheme 2. Oligo Homo-Trp Model System, Where $n = 4\text{--}7$ ^a



^aMercaptopropionic acid modification allowed oriented monolayer formation on gold substrate.

effective charge mediator in nature, and various examples exist in the literature for its involvement in intra- and interprotein charge transfer.³¹ Therefore, it can serve as a good benchmark system for this study. Figure 3a shows the ETp as a function of the peptide length, changed by varying the number of repeating Trp units. While Trp monolayers generally facilitate high conductance, the ETp rate decreased gradually with the peptide's length. This is expected, as the electrode separation distance dictates conduction. A closer examination of the ETp magnitude reveals that the currents' dependence on the peptide length is close to exponential (Figure 3b), which suggests tunneling, with a tunneling barrier height that is independent of peptide length. From this exponential dependence we calculated a decay constant of $\beta = 0.58 \pm 0.06 \text{ \AA}^{-1}$. This value is independent of temperature (Figure 3c). This behavior may suggest off-resonance tunneling as the dominant conduction mechanism. Such a mechanism can be operative if the energy levels that affect ETp differ by several kT (where k is the Boltzmann constant and T the absolute temperature) from those of the electrodes' Fermi levels. Our results are in good agreement with previous solid-state ETp measurements performed using conjugated molecules.³² The calculated value of $\beta = 0.58 \pm 0.06 \text{ \AA}^{-1}$ is slightly smaller than that for the commonly reported values of fully saturated molecules ($0.8\text{--}1 \text{ \AA}^{-1}$)³³ and higher than that for conjugated ones ($0.2\text{--}0.6 \text{ \AA}^{-1}$).^{34,35} This is reasonable, given that the length decay constant is a value that also depends on the energy levels of the donor and acceptor, in our case, the Fermi level of the gold substrate and gold nanorod electrodes.

Figure 4a shows the computed gas-phase eigenvalue spectra of several extended homo-Trp with $n = 1, 4\text{--}7$ and the corresponding HOMO and LUMO orbitals. As a verification for the accuracy of our computational method, the HOMO value of -7.8 eV, calculated for a single Trp unit, agrees well with previously reported experimental ultraviolet photo-emission spectroscopy values for the ionization energy of a single Trp amino-acid in the gas phase, $\sim 7.8\text{--}7.9$ eV.³⁷ Our results show that the changes in the frontier energy levels with peptide length, though not negligible, are relatively small (up to

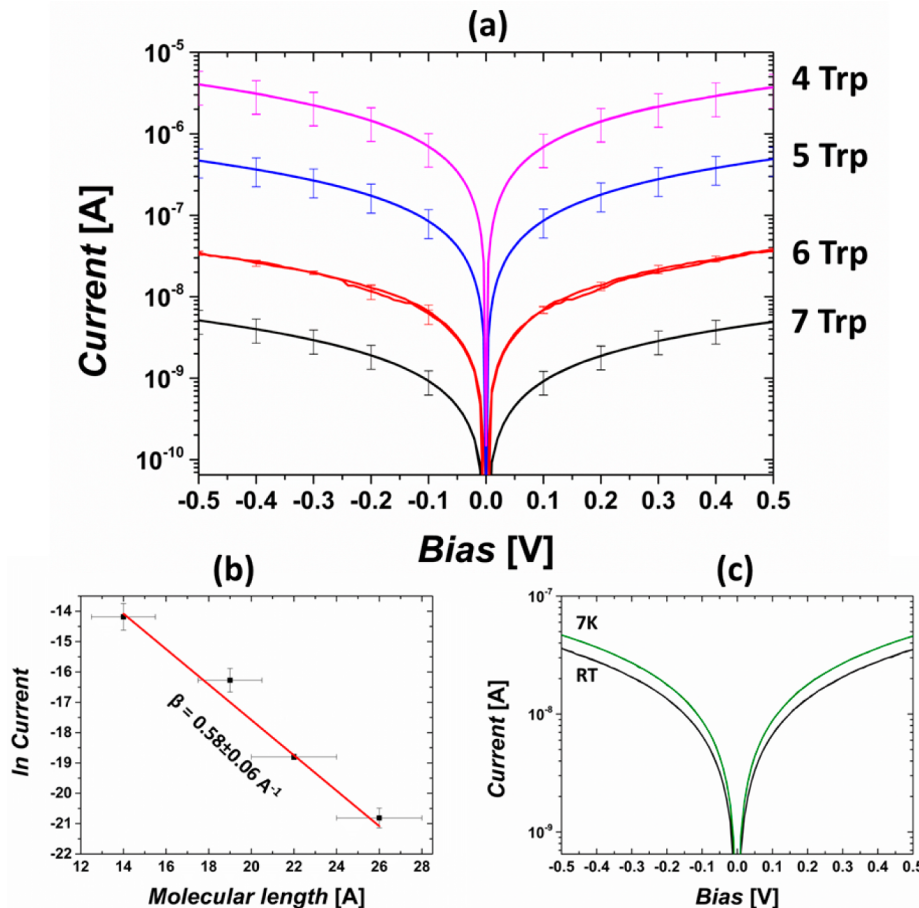


Figure 3. (a) Current–voltage plots of 4- to 7-mer homo-Trp monolayer junctions. (b) Plot of $\ln(\text{current})$ at $+0.1$ V applied bias vs monolayer thickness, the slope of which yields the length decay parameter, $\beta = 0.58 \pm 0.06 \text{ Å}^{-1}$. (c) Current–voltage plots of hexa-Trp at 7K and 300 K. The slight current increase with decreasing temperature maybe due to a lower defect density with decreasing temperature, as was found for alkyl chain monolayers.³⁶

0.55 eV for the HOMO level and 0.8 eV for the unbound LUMO level). This can explain the experimental observation that indicates an exponential dependence of the current on peptide length, with a tunneling barrier height for ETp that does not change significantly with the length of homo-Trp.

The above finding may appear surprising at first glance, as it is common to relate larger molecular systems with smaller ionization potentials. To explain this, Figure 4a also shows the HOMO orbital densities of the homo-Trp at different lengths. These are localized on one of the aromatic indole side-chains, typically on the one closest to the peptide C-terminus, but not always. A similar localization occurs for the LUMO levels, but for the peptide N-terminus. This side preference likely arises from the molecular dipole orientation,^{18,19} pointing from the N-terminus to the C-terminus. The fact that the orbitals are highly localized explains the small difference between the HOMO levels of the different Trp peptides, as the energies are being determined by a very similar charge-distribution, almost independent of peptide length. Still, one then has to explain how efficient tunneling may proceed without effective charge delocalization along the molecular bridge. In this specific case, while the HOMO level is indeed very localized, the HOMO band, namely the combination of the HOMO to HOMO–7 levels, is delocalized over the peptide (Figure 4b), as each of the levels is localized on a different side-chain (and constitutes the HOMO level of a specific single indole ring), and the sum of

these charge densities is delocalized over the entire molecule. A similar observation was made by Wolak et al.³⁸ for peptide nucleic acids (PNA) on Au. However, it should be noted that if the transport mechanism is tunneling, localized charge distributions could still be considered, with lower efficiencies than those obtainable with delocalized distributions.²⁸

As mentioned above, upon shifting from the gas phase to a solid-state monolayer that is adsorbed on a metal surface, two main effects are expected to change the energy levels: First, dipole–dipole interactions between the peptides can occur. It has been shown^{19,25} that this dipole effect lowers the energy gap and shifts the occupied (unoccupied) spectra to higher (lower) energies. Second, as already mentioned above, if the monolayer is bound to a Au surface, the molecular energy levels are expected to further renormalize due to surface polarization and shift caused by surface dipole effects.²³ This latter effect is not expected to be strongly dependent on the peptide length. Therefore, we expect the energy barrier height, measured for transport through a solid-state junction, to converge as the number of Trp in the peptide increases. The same trend is observed by comparing 4Ala with 7Ala (see Figure S6 in SI).

The Effect of Secondary Structure on Electronic Transport via Homopeptide Monolayers. We studied the effect of secondary structure by comparing the ETp via monolayer junctions of extended and helical Ala and Lys homopeptides. We compare ETp via the extended hepta-Ala

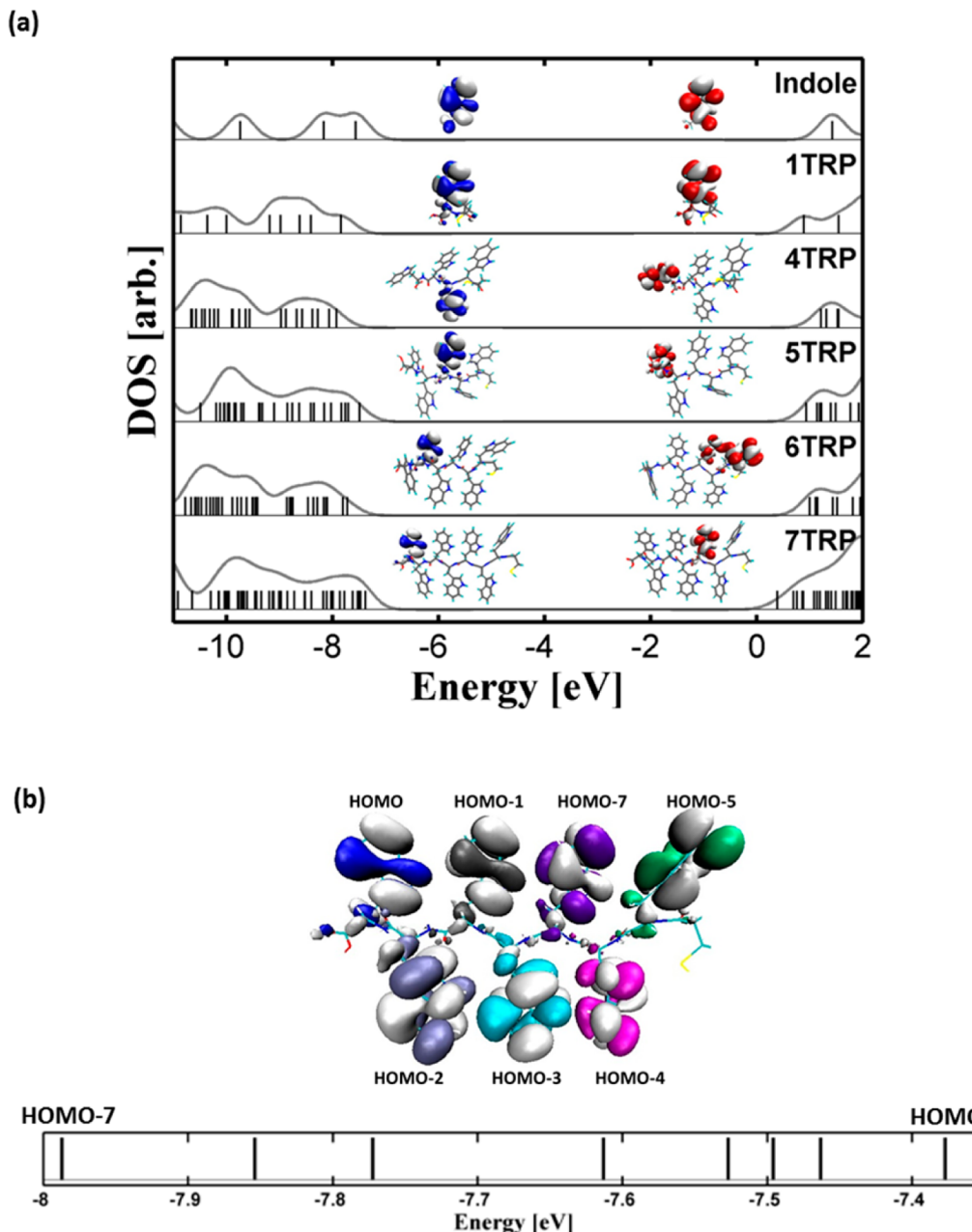


Figure 4. (a) Electronic structure calculations of an indole ring and an *n*-mer Trp in the gas phase, using DFT within the OT-RSH scheme. The geometrical properties were obtained from MD simulations (see SI). HOMO and LUMO orbitals are designated in blue and red, respectively. (b) Superposition of HOMO to HOMO-7 of hepta-Trp, indicating delocalization over the whole peptide within a relatively narrow range of ionization energies of 0.6 eV, emphasized by the bottom energy scale, from the HOMO level around -7.4 eV until the HOMO-7 level at ~ -8 eV. The energy values shown for the different orbitals are absolute (with the vacuum level = 0), with an estimated accuracy of ~0.2 eV.

and hepta-Lys, examined above, to 20-mer Ala and 20-mer Lys (neutral), which have a high propensity to form a helix. The lengths of the 20-mer helices, as deduced from ellipsometry, were 29–30 Å (see Table 1), i.e., ~4 Å longer than the respective extended hepta-peptides (see Table S1 in the SI for estimated footprint areas of the 20mers). Nevertheless, Figure 5a shows that the observed conduction via the helices was not smaller, as expected from length alone, but in fact was substantially higher than via the extended peptides. Current–voltage curves determined between 20 and 260 K show a weak temperature dependence above ~70 K (Figure 5b,c), in good agreement with the ET observed by Chance and DeVault³⁹ and, more recently, by some of us for solid-state conduction

across protein junctions.⁴⁰ The calculated activation energies (10–15 meV, 1–1.5 kJ/mol) are comparable to those, obtained by us for transport via several mutants of (predominantly helical) Cyt C, bound covalently to one of the contacting electrodes,⁴⁰ as is the case here for 20 Ala.

To try and rationalize the observed differences in conductance caused by the change in secondary structure, we computed the electronic energy levels of the Ala peptides in different conformations. Figure 6 shows that the computed frontier orbital energy levels of extended Ala with 1, 7, and 20 repeating units (denoted in the Figure as 1Ala, 7Ala, and 20Ala-L, respectively) differ from each other only by up to 0.15 eV. Like in the case of Trp, this is due to the highly localized nature

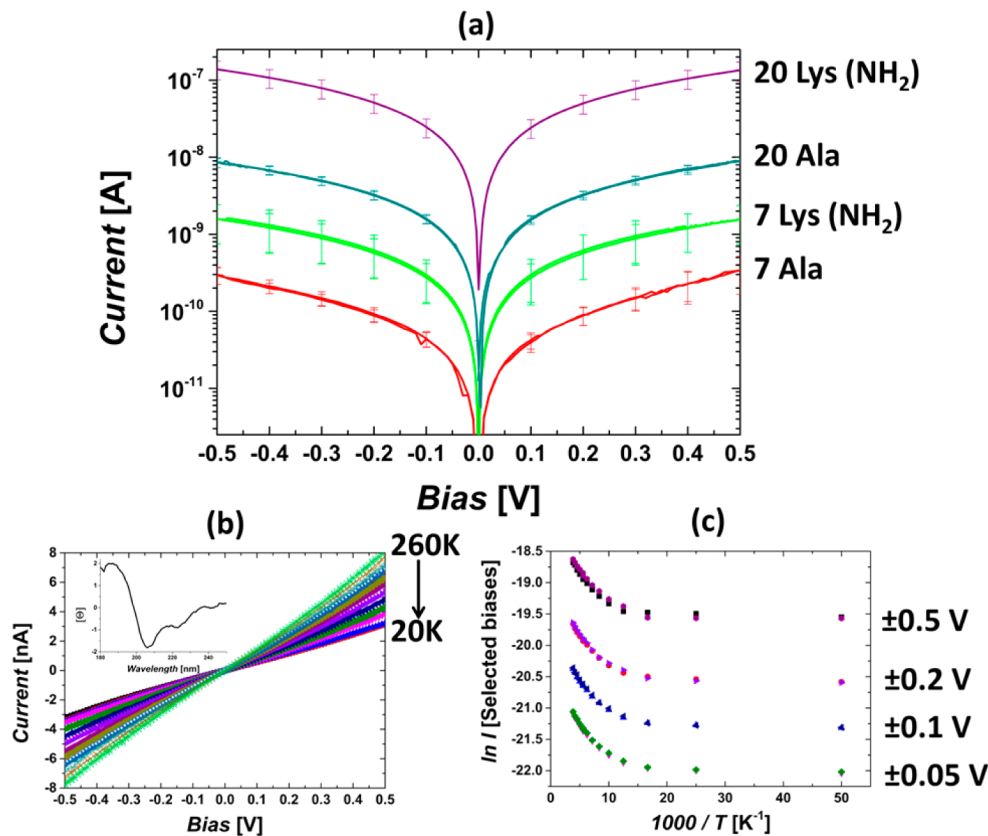


Figure 5. (a) Comparison of current–voltage curves measured via homo-Ala and homo-Lys monolayers in an extended conformation (7-mer, 25 Å) and a helical conformation (20-mer, 29 Å) at room temperature. (b) Current–voltage plots of 20-mer Ala from 20 to 260 K; (inset): circular dichroism spectrum showing helical signature of the 20-mer Ala in a hexafluoro-2-propanol solution. (c) $\ln(I)$ as a function of temperature (plotted as $1000/T$) from (b), at selected biases.

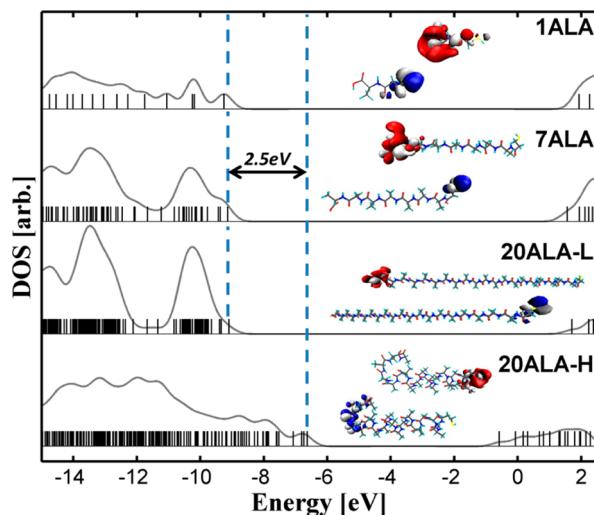


Figure 6. Density of states, as a function of energy for different configurations of the homo-Ala peptide, with different numbers of repeating units and their secondary structure. HOMO and LUMO are designated in blue and red, respectively. 20Ala-L and 20Ala-H refer to homopeptides with extended and helical structure, respectively.

of the charge distribution. The unbound LUMO levels show the same similarity for the extended peptides. However, the HOMO level of the helical 20-Ala (denoted as 20Ala-H) is 2.5 eV higher in energy than the HOMO levels of the extended 20 and 7Ala, and the LUMO level is lower by ~2 eV and bound

(i.e., below the vacuum level). These observations suggest an immediate connection between the ETp via a peptide and its secondary structure, suggesting a much lower barrier height for transport via the helical peptide.

An examination of the frontier orbitals, also shown in Figure 6, reveals a charge distribution that is more delocalized in the helical structure than in the extended one. This result is in agreement with previously reported calculations on helical structures performed using conventional DFT hybrid functionals.^{30,41,42}

Combining the experimental observations with the electronic structure gas phase calculations (summarized in Table 1) leads us to suggest the following: Upon helix formation, a decrease occurs in the HOMO–LUMO gap, compared to that of the extended structure, and the charge is distributed over a larger fraction of the molecule than in the case of extended peptides. The empirical decay constant between the donor and acceptor (also between two Au electrodes, as in this case) can be formulated as⁴³

$$\beta = \frac{-2}{\delta} \ln \left(\frac{h_{bb}}{\Delta E} \right) \quad (1)$$

where h_{bb} is the electronic coupling between adjacent units in the bridge, δ is the length of the bridge elements (in our case the different amino acids), and ΔE is the barrier height. Therefore, we suggest that helical structures support long-range electronic transport due to a lower barrier (ΔE) and possibly also an increase in the electronic coupling (h_{bb}) within the peptide. This results from the more delocalized distribution of

the outer-valence states in the helical form than in the extended one. However, it is important to note that due to the large helical dipole, there is no full delocalization along the molecular bridge for at least few eV below the HOMO level, unlike in the case of extended Trp peptide, shown above in Figure 4b.

■ DISCUSSION

Our results show a direct relation between structural properties and charge transport through homopeptides, measured as monolayers. Specifically, we find that different amino acids exhibit distinct ET_p efficiencies, in correlation with their predicted frontier energy levels in the gas-phase. Naturally, the transition from gas-phase to a solid-state environment changes the energy levels of each peptide (usually this will bring them closer to the Fermi level of the electrodes)⁴⁴ due to some charge transfer at the interface and dipole–dipole interactions within the monolayer. The transition from calculating the gas phase peptides to calculating the actual solid-state junction within the same high level of accuracy, so as to examine the effect of the different environments on the electronic coupling, is an important issue which we intend to investigate further. However, we do expect the calculated solid-state energy levels to follow similar trends to those, calculated for the peptides in the gas-phase.

Our findings contribute additional insights to existing models of tunneling pathways and average packing density for ET and conduction through proteins.^{45,46} Both models rely on the reasonable assumption that electronic interactions decay much more rapidly through space than through bond. We introduce here an analysis in which the chemical nature and structure of the peptide affects the entire coupling matrix element. This notion is based on the different ET_p efficiency measured via different homopeptides with similar conformations, where the ET_p dependence on amino acid composition is conserved in both extended and helical conformation.

In addition, we showed that the conduction through extended hepta-peptides is largely affected by the overall charge of their side-chains. Previous results by Xiao et al.⁴⁷ indicated that ET_p efficiency increases upon protonation of the peptide's amino side chain. Gao et al. reported a notable effect on ET efficiency upon protonation of amino side chains, which can be increased or decreased, depending on the contribution of the Coulomb repulsion energy to the activation energy for ET in the system.⁴⁸ However, this is valid for ET reactions, which can be rationalized by Marcus theory. In the present case, which resembles more the work done by Xiao et al., we also considered that the presence of positive charge on the Lys residue can induce LUMO-mediated transport and may explain the lower conductance via deprotonated Glu by the charge localization.

The exponential decrease in the current across a junction with extended homo-Trp of varying length and the fact that it does not depend significantly on temperature are strong indications that a tunneling transport mechanism, most likely off-resonance, is the dominant one for extended peptides junctions (see Figure 3b,c). Other theoretical work predicted that in the extended conformation both electrons and holes may contribute to the conductance/transfer, while hole transport (and transfer) is the dominant ET_p mechanism via a helical peptide structure.⁴⁹ Here, we chose to focus on the peptide's HOMO levels, but a similar interpretation emerges when the LUMO levels are examined.

The main conclusion from our work is that the contribution of the side chains to the tunneling barrier height adds to other parameters that control ET_p and ET such as the peptide secondary structure,⁵⁰ dipole,^{51–54} and dynamics.^{55–59} For example, the ratio of ET_p at room temperature via extended hepta-Trp and hepta-Ala is ≈20 (Figure 1). The molecular diameter of Ala is smaller than that of the other peptides (by a factor of 3–4; see atomistic modeling section in the SI). Hence, the density of the Ala homopeptides' monolayers can be 10–15 times higher than that of the monolayers, made with the other peptides. Hence, the measured lower currents via Ala peptide junctions, compared to Trp junctions, actually present an upper limit ET_p via Ala. At equal density of molecules the difference may even be larger by an order of magnitude. The difference in theoretical monolayer density between 7- and 20-mer Ala peptides is at most a factor of 2.

Secondary structure formation can further facilitate ET_p, as a ratio of up to 400 in ET_p efficiency was observed between helical and extended homo-Ala peptides (Figure 5).

Assuming the operation of an off-resonance tunneling mechanism, we can use the conduction ratios to estimate a change in ET_p efficiency of up to $\Delta\beta \approx 0.1 \text{ \AA}^{-1}$ by different sequences (in the same secondary structure) and up to $\Delta\beta = 0.20–0.25 \text{ \AA}^{-1}$ by combined different secondary structures and sequences, for a 25 Å polypeptide (for the detailed calculation see SI).

Our data show a connection with results of ET_p measurements via different Cyt C mutants that were covalently bound to an electrode and that showed similar low activation energies at elevated temperatures.

We note that our experimental results do not provide clear indications for operation of a hopping transport mechanism, because the latter is a thermally activated process, reflecting the (partial) residence of the charge on the bridge. Present experimental observations show temperature-independent transport, except for the helical peptides, which exhibit very low activation energies (Figure 5). Thus, any residence of charge on the peptide's amide bonds, allowing them to serve as relay stations, will be minimal. Indeed our theoretical results agree with this, in terms of the absence of localization of charge on the backbone. This is relevant as hopping transport is commonly correlated with HOMO (or LUMO) levels that are localized on the presumed conduction path. We suggest that the reason for more efficient conduction via helical than via extended peptide conformations is a substantial change in level alignment, possibly together with changes in (de)localization trends.

■ SUMMARY OF MATERIALS AND METHODS

All peptides, extended and helical, were incubated for approximately 48 h on a gold-coated (50 nm) highly doped P⁺⁺-Si slides. The concentration of the peptide in solution was 0.2–0.5 mM, which enabled the formation of a self-assembled monolayer via the reaction of the SH terminal of the mercaptopropionic acid linker with the Au surface, to form S–Au bonds via MPA. Immediately after monolayer formation, samples were washed, dried, and characterized by ellipsometry and polarization-modulated, infra-red, reflection adsorption spectroscopy, PM-IRRAS (see further explanation in the SI). A different configuration was used for fabricating the molecular junctions for transport measurements. In brief, Au electrodes were fabricated on top of Si wafer by using photolithography, yielding a substrate that contains 260 devices. This was then used to bring a single Au nanorod to bridge between two electrodes, as reported previously.¹¹ The peptides were immobilized on the wafer in the same conditions as

above (using the same basic chemistry to enable Au–S bond formation). After monolayer formation, gold nanorods were dielectrophoretically trapped to close the circuit^{11,60} (see Scheme 1; for further explanation see SI). The final architecture of all measured junctions is similar to the configuration shown in Scheme 1, with only a single Au nanorod as a top contact. Since the yield of trapping was low, ~7%, the occasion of two or more Au nanorods bridging between two contact pads was rather rare and could be easily detected using an optical microscope, prior to the electronic transport measurements themselves.

Next, the samples were loaded on an electrically floating sample stage and placed in a cryogenic Lakeshore probe station (TTPX). Current–voltage (*I*–*V*) measurements were performed to assess the transport efficiency across peptide monolayers, using a Keithley 6430 Sub-Femtoamp Source-Meter, with a voltage scan rate of 20 mV/s. For all measurements, a specific side of the junction was grounded, while the other one was biased, in a consistent manner (in order to ensure that the bias polarity was in the same direction for all measurements). In each set of experiments, scans were acquired that started and ended at 0 V (i.e., voltage sweep was 0 → −0.5 V, −0.5 V → 0.5 V, 0.5 V → 0 V), to check if features in the *I*–*V* behavior originate from the polarity of the initial voltage that is applied and from the scan direction (hysteresis check). Vacuum conditions were 10^{−4}–10^{−6} mbar (depending on temperature). Due to the mesoscopic nature of the junction, the error in currents was large (~2 order of magnitude). However, about 60–70% of the junctions, measured by *I*–*V* and IETS, did not show the expected Au–S vibrational mode and revealed high current magnitude. Hence, only junctions containing peptides that were identified to immobilize via the Au–S bond and that were not partially shorted were further analyzed in the current–voltage distribution, and the error of these junctions are shown in Figure 1b.

For differential conductance and IETS measurements, two lock-in amplifiers were added, and their output was measured simultaneously with that of the current–voltage (for full description see SI).

■ ASSOCIATED CONTENT

S Supporting Information

Preparation of peptide monolayers, atomistic modeling of the peptide monolayers mesoscopic Au nanorod top contact formation, current–voltage (*I*–*V*) measurements, differential conductance and IETS measurements at 7 K, DFT and electronic structure calculations of all peptides, theoretical calculations of (de)protonation effects of side chains. In addition extracted decay constant from homo-Trp and homo-Ala are presented together with an estimation of ETp barrier height via homo -Trp. Video S1 depicting IETS of hepta-Glu monolayer in a solid-state junction. The Supporting Information is available free of charge on the ACS Publications website at DOI: [10.1021/jacs.5b03933](https://doi.org/10.1021/jacs.5b03933).

■ AUTHOR INFORMATION

Corresponding Authors

*david.cahen@weizmann.ac.il

*mudi.sheves@weizmann.ac.il

Present Address

¹Department of Chemistry, Physical, and Theoretical Chemistry Laboratory, Oxford University, South Parks Road, Oxford OX1 3QZ, United Kingdom

Notes

The authors declare no competing financial interest.

■ ACKNOWLEDGMENTS

We would like to thank Y. Selzer and R. Arielly for sharing the expertise of preparing and trapping suspended Au nanorods for a mesoscopic electrical top contact, A. Nitzan and A. Vilan for

guiding notes regarding transport mechanisms and data interpretation, Y. Selzer, K. L. Narasimhan and D. A. Egger for illuminating discussions on the electronic structure calculations. We are grateful to the Minerva Foundation, Munich (D.C., M.S., I.P.), the Nancy and Stephen Grand Centre for Sensors and Security (D.C.), the Kimmelman center for Biomolecular Structure and Assembly (M.S.), the Israel Science Foundation (L.K., D.C.), the European Research Council (L.K.), and the Lise Meitner Minerva Center for Computational Chemistry (L.K.) for support. L.S. thanks the Israeli Ministry of Science for an Eshkol Ph.D scholarship. R.L. is grateful to the European Union for a Marie Curie postdoctoral fellowship (Grant FP7-PEOPLE-2011-IEF no. 298664). S.R.A. acknowledges support by an Adams fellowship of the Israel Academy of Sciences and Humanities. Y.L. holds the Morton and Gladys Pickman professional chair in Structural Biology. M.S. holds the Katzir-Makineni chair in Chemistry. D.C. holds the Rowland and Sylvia Schaefer Chair in Energy Research.

■ REFERENCES

- Gray, H. B.; Winkler, J. R. *Annu. Rev. Biochem.* **1996**, *65* (1), 537.
- Wei, J. J.; Liu, H.; Niki, K.; Margoliash, E.; Waldeck, D. H. *J. Phys. Chem. B* **2004**, *108* (43), 16912.
- Alessandrinini, A.; Corni, S.; Facci, P. *Phys. Chem. Chem. Phys.* **2006**, *8* (38), 4383.
- Davis, J. J.; Wrathmell, C. L.; Zhao, J.; Fletcher, J. *J. Mol. Recognit.* **2004**, *17* (3), 167.
- Ron, I.; Sepunaru, L.; Itzhakov, S.; Belenkova, T.; Friedman, N.; Pecht, I.; Sheves, M.; Cahen, D. *J. Am. Chem. Soc.* **2010**, *132* (12), 4131.
- Pia, E. A. D.; Chi, Q.; Jones, D. D.; Macdonald, J. E.; Ulstrup, J.; Elliott, M. *Nano Lett.* **2011**, *11* (1), 176.
- Atanassov, A.; Hendl, Z.; Berkovich, I.; Ashkenasy, G.; Ashkenasy, N. *Biopolymers* **2013**, *100* (1), 93.
- Sek, S. *Biopolymers* **2013**, *100* (1), 71.
- Long, Y.-T.; Abu-Irhayem, E.; Kraatz, H.-B. *Chem. - Eur. J.* **2005**, *11* (18), 5186.
- Juhaniwicz, J.; Sek, S. *J. Electroanal. Chem.* **2010**, *649* (1–2), 83.
- Noy, G.; Ophir, A.; Selzer, Y. *Angew. Chem.* **2010**, *122* (33), 5870.
- Kronik, L.; Stein, T.; Refaeli-Abramson, S.; Baer, R. *J. Chem. Theory Comput.* **2012**, *8* (5), 1515.
- Stein, T.; Eisenberg, H.; Kronik, L.; Baer, R. *Phys. Rev. Lett.* **2010**, *105* (26), 266802.
- Refaeli-Abramson, S.; Sharifzadeh, S.; Govind, N.; Autschbach, J.; Neaton, J. B.; Baer, R.; Kronik, L. *Phys. Rev. Lett.* **2012**, *109* (22), 226405.
- Egger, D. A.; Weissman, S.; Refaeli-Abramson, S.; Sharifzadeh, S.; Dauth, M.; Baer, R.; Kümmel, S.; Neaton, J. B.; Zoher, E.; Kronik, L. *J. Chem. Theory Comput.* **2014**, *10* (5), 1934.
- Lüftner, D.; Refaeli-Abramson, S.; Pachler, M.; Resel, R.; Ramsey, M. G.; Kronik, L.; Puschnig, P. *Phys. Rev. B: Condens. Matter Mater. Phys.* **2014**, *90* (7), 075204.
- Rudberg, E. *J. Phys.: Condens. Matter* **2012**, *24* (7), 072202.
- Lever, G.; Cole, D. J.; Hine, N. D. M.; Haynes, P. D.; Payne, M. C. *J. Phys.: Condens. Matter* **2013**, *25* (15), 152101.
- Rissner, F.; Natan, A.; Egger, D. A.; Hofmann, O. T.; Kronik, L.; Zoher, E. *Org. Electron.* **2012**, *13* (12), 3165.
- Okabayashi, N.; Konda, Y.; Komeda, T. *Phys. Rev. Lett.* **2008**, *100* (21), 217801.
- Giraud, G.; Karolin, J.; Wynne, K. *Biophys. J.* **2003**, *85* (3), 1903.
- Kim, Y.; Hellmuth, T. J.; Bürkle, M.; Pauly, F.; Scheer, E. *ACS Nano* **2011**, *5* (5), 4104.
- Neaton, J. B.; Hybertsen, M. S.; Louie, S. G. *Phys. Rev. Lett.* **2006**, *97* (21), 216405.

- (24) Heimel, G.; Romaner, L.; Brédas, J.-L.; Zoyer, E. *Phys. Rev. Lett.* **2006**, *96* (19), 196806.
- (25) Rissner, F.; Egger, D. A.; Natan, A.; Körzdörfer, T.; Kümmel, S.; Kronik, L.; Zoyer, E. *J. Am. Chem. Soc.* **2011**, *133* (46), 18634.
- (26) Simmons, J. G. *J. Appl. Phys.* **1963**, *34* (6), 1793.
- (27) Landauer, R. *IBM J. Res. Dev.* **1957**, *1* (3), 223.
- (28) Cuevas, J. C.; Scheer, E. *Molecular Electronics: An Introduction to Theory and Experiment*; World Scientific: Singapore, 2010.
- (29) Heimel, G.; Romaner, L.; Zoyer, E.; Brédas, J.-L. *Nano Lett.* **2007**, *7* (4), 932.
- (30) Tarakeshwar, P.; Palma, J. L.; Holland, G. P.; Fromme, P.; Yarger, J. L.; Mujica, V. *J. Phys. Chem. Lett.* **2014**, *5* (20), 3555.
- (31) Faraggi, M.; DeFelippis, M. R.; Klapper, M. H. *J. Am. Chem. Soc.* **1989**, *111* (14), 5141.
- (32) Choi, S. H.; Risko, C.; Delgado, M. C. R.; Kim, B.; Brédas, J.-L.; Frisbie, C. D. *J. Am. Chem. Soc.* **2010**, *132* (12), 4358.
- (33) Yaffe, O.; Qi, Y.; Scheres, L.; Puniredd, S. R.; Segev, L.; Ely, T.; Haick, H.; Zuilhof, H.; Vilan, A.; Kronik, L.; Kahn, A.; Cahen, D. *Phys. Rev. B: Condens. Matter Mater. Phys.* **2012**, *85* (4), 045433.
- (34) Salomon, A.; Cahen, D.; Lindsay, S.; Tomfohr, J.; Engelkes, V. b.; Frisbie, C. d. *Adv. Mater.* **2003**, *15* (22), 1881.
- (35) Holmlin, R. E.; Haag, R.; Chabinyc, M. L.; Ismagilov, R. F.; Cohen, A. E.; Terfort, A.; Rampi, M. A.; Whitesides, G. M. *J. Am. Chem. Soc.* **2001**, *123* (21), 5075.
- (36) Shpaisman, H.; Seitz, O.; Yaffe, O.; Roodenko, K.; Scheres, L.; Zuilhof, H.; Chabal, Y. J.; Sueyoshi, T.; Kera, S.; Ueno, N.; Vilan, A.; Cahen, D. *Chem. Sci.* **2012**, *3* (3), 851.
- (37) Cannington, P. H.; Ham, N. S. *J. Electron Spectrosc. Relat. Phenom.* **1979**, *15* (1), 79.
- (38) Wolak, M. A.; Balaeff, A.; Gutmann, S.; Helmrich, H. J.; Vosloo, R.; Beerbohm, M. M.; Wierzbinski, E.; Waldeck, D. H.; Bezer, S.; Achim, C.; Beratan, D. N.; Schlaf, R. *J. Phys. Chem. C* **2011**, *115* (34), 17123.
- (39) De Vault, D.; Chance, B. *Biophys. J.* **1966**, *6* (6), 825.
- (40) Amdursky, N.; Ferber, D.; Bortolotti, C. A.; Dolgikh, D. A.; Chertkova, R. V.; Pecht, I.; Sheves, M.; Cahen, D. *Proc. Natl. Acad. Sci. U. S. A.* **2014**, *111* (15), 5556.
- (41) Chen, X.; Zhang, L.; Zhang, L.; Sun, W.; Zhang, Z.; Liu, H.; Bu, Y.; Cukier, R. I. *J. Phys. Chem. Lett.* **2010**, *1* (10), 1637.
- (42) Li, X.; Yu, S.; Yang, M.; Xu, C.; Wang, Y.; Chen, L. *Phys. E (Amsterdam, Neth.)* **2014**, *57*, 63.
- (43) Joachim, C.; Ratner, M. A. *Nanotechnology* **2004**, *15* (8), 1065.
- (44) Zahid, F.; Paulsson, M.; Datta, S. Electrical Conduction through Molecules. In *Advanced Semiconductors and Organic Nano-Techniques*; H. Morkoc Academic Press: London, 2003.
- (45) Moser, C. C.; Page, C. C.; Chen, X.; Dutton, P. L. *JBIC, J. Biol. Inorg. Chem.* **1997**, *2* (3), 393.
- (46) Onuchic, J. N.; Beratan, D. N.; Winkler, J. R.; Gray, H. B. *Annu. Rev. Biophys. Biomol. Struct.* **1992**, *21* (1), 349.
- (47) Xiao; Xu; Tao. *J. Am. Chem. Soc.* **2004**, *126* (17), 5370.
- (48) Gao, J.; Müller, P.; Wang, M.; Eckhardt, S.; Lauz, M.; Fromm, K. M.; Giese, B. *Angew. Chem., Int. Ed.* **2011**, *50* (8), 1926.
- (49) Wolfgang, J.; Risser, S. M.; Priyadarshy, S.; Beratan, D. N. *J. Phys. Chem. B* **1997**, *101* (15), 2986.
- (50) Shin, Y. K.; Newton, M. D.; Isied, S. S. *J. Am. Chem. Soc.* **2003**, *125* (13), 3722.
- (51) Carmeli, I.; Naaman, R.; Leitus, G.; Reich, S.; Vager, Z. *Isr. J. Chem.* **2003**, *43* (3–4), 399.
- (52) Shlizerman, C.; Atanassov, A.; Berkovich, I.; Ashkenasy, G.; Ashkenasy, N. *J. Am. Chem. Soc.* **2010**, *132* (14), 5070.
- (53) Becucci, L.; Guryanov, I.; Maran, F.; Guidelli, R. *J. Am. Chem. Soc.* **2010**, *132* (17), 6194.
- (54) Lauz, M.; Eckhardt, S.; Fromm, K. M.; Giese, B. *Phys. Chem. Chem. Phys.* **2012**, *14* (40), 13785.
- (55) Jortner, J.; Bixon, M. *Mol. Cryst. Liq. Cryst. Sci. Technol., Sect. A* **1993**, *234* (1), 29.
- (56) Beratan, D. N.; Liu, C.; Migliore, A.; Polizzi, N. F.; Skourtis, S.; Zhang, P.; Zhang, Y. *Acc. Chem. Res.* **2015**, *48* (2), 474.
- (57) Skourtis, S. S.; Waldeck, D. H.; Beratan, D. N. *Annu. Rev. Phys. Chem.* **2010**, *61* (1), 461.
- (58) Mandal, H. S.; Kraatz, H.-B. *Chem. Phys.* **2006**, *326* (1), 246.
- (59) Schlag, E. W.; Sheu, S.-Y.; Yang, D.-Y.; Selzle, H. L.; Lin, S. H. *Proc. Natl. Acad. Sci. U. S. A.* **2000**, *97* (3), 1068.
- (60) Evoy, S.; DiLello, N.; Deshpande, V.; Narayanan, A.; Liu, H.; Riegelman, M.; Martin, B. R.; Hailer, B.; Bradley, J.-C.; Weiss, W.; Mayer, T. S.; Gogotsi, Y.; Bau, H. H.; Mallouk, T. E.; Raman, S. *Microelectron. Eng.* **2004**, *75* (1), 31.